Relative Navigation of High-Altitude Spacecraft Using Dual-Frequency Civilian CDGPS

by Mark L. Psiaki and Shan Mohiuddin
Cornell University

BIOGRAPHIES

Mark L. Psiaki is an Associate Professor of Mechanical and Aerospace Engineering. He received a B.A. in Physics and M.A. and Ph.D. degrees in Mechanical and Aerospace Engineering from Princeton University. His research interests are in the areas of estimation and filtering, spacecraft attitude and orbit determination, and GPS technology and applications.

Shan Mohiuddin is a graduate student in Mechanical and Aerospace Engineering. He received a B.S. in Aerospace Engineering from Virginia Tech in 2003. He spent the summer of 2003 working in the Flight Dynamics Analysis Branch at the NASA/Goddard Space Flight Center. His research focuses on developing estimation techniques for precise spacecraft relative navigation, on general GPS data processing algorithms, and on GPS receiver design.

ABSTRACT

Carrier-phase differential GPS techniques are used to perform high accuracy relative position estimation for pairs of spacecraft that orbit at altitudes above the GPS constellation. These techniques are being developed in support of planned high-altitude missions that make high resolution science measurements by using data from sensors aboard formations of spacecraft. Precise knowledge of relative spacecraft positions within a formation constitutes a key ingredient needed for feedback control of the formation or for processing of its science data. Kinematic techniques are developed to determine relative position. They use dual-frequency signals to remove ionospheric effects, and they use LAMBDA/integer-least-squares methods to estimate double-differenced carrier phase ambiguities. A truth-model simulation is used to evaluate the performance of this system at high altitudes. In geosynchronous Earth orbit, the system can resolve ambiguities almost instantaneously, and it can achieve relative position accuracies of about 0.25 m over short baselines. At an altitude of 17 Earth radii, the resolution of ambiguities requires on the order of 500 sec, relative position accuracies degrade to about 10 m, and intermittent ambiguity errors occur on a small subset of the tracked signals. The largest relative position errors are in the altitude direction and result from the large GDOP values that are caused by having all available GPS satellites below the user spacecraft.

INTRODUCTION

Missions that employ formations of spacecraft are currently being considered [1]. Formation-based interferometry can be used to achieve performance comparable to that of a single large reflective mirror for missions that study the cosmos using optical wavelengths or that monitor the Earth using radar. A planned science application will use a formation of 4 satellites grouped about a highly elliptical mean orbit in order to study the Earth's magnetosphere [2].

An important part of formation flying is the determination of the relative positions of the formation's component spacecraft. Carrier phase differential GPS (CDGPS) techniques have the potential to deliver accuracies on the order of 1 cm and to operate autonomously. This potential has been verified by simulation and by post processing of flight data for formations that operate in low Earth orbit (LEO) [3-7].

A new goal is to extend the applicability of formation flying CDGPS techniques to altitudes above the LEO domain. Geosynchronous (GEO) formations are useful for many Earth observing applications, and high-altitude Earth orbits (HEO), which lie above GEO, are useful for science applications [1]. Reference 8 discusses the usefulness of absolute GPS techniques as aids to the operation for some of NASA's planned Lunar exploration missions. The use of CDGPS techniques at Lunar altitudes, if feasible, might further aid such systems.

Three significant challenges must be met in order to use CDGPS techniques at high altitudes. A user spacecraft falls outside the main transmission lobes of more and more GPS satellites as its altitude increases above about 3000 km. CDGPS techniques usually require tracking of 5 or more signals. The use of weak signals in the transmission antennas' side lobes can increase the number of available GPS satellites and thereby enable the use of CDGPS techniques in these situations. Therefore, high-altitude CDGPS can be implemented only if the user

Preprint from ION GNSS 2005

receivers implement weak-signal acquisition and tracking techniques, as described in Refs. 9-12. The present study presumes the availability and use of receivers that employ weak-signal technology [*]. It also presumes the availability of the GPS signals' navigation data bits, obtained either through a separate data link or though "voting" of bit values over multiple repeated data frames.

The second challenge is that of high geometric dilution of precision (GDOP). The available GPS satellites are grouped close together around the nadir direction when viewed from a high altitude. This grouping produces GDOP values on the order of 10 in GEO, 100 at a HEO altitude of 17 Earth radii, and 1000 at Lunar altitudes if the user receiver can process weak side-lobe signals. The potential problem for CDGPS techniques is that the double-differenced carrier phase ambiguities may not be resolvable as integers. If the integers can be resolved, then the relative position estimation errors will be very small, on the order of GDOP$\times l \times s_f$, where l is the carrier wavelength and s_f is the carrier phase measurement error standard deviation; $l \times s_f$ is normally on the order of 1 cm. If GDOP is large, then GDOP$\times s_f$ will be on the order of half a wavelength or more. Intuition implies that errors larger than half a wavelength would preclude the correct resolution of carrier cycle ambiguities as exact integers. A failure to resolve the ambiguities as integers would increase the relative position errors far beyond GDOP$\times l \times s_f$. Therefore, it is hoped that intuition is wrong in this case.

The third challenge is that of slow rates of change in the directions of the line-of-sight (LOS) vectors from the user spacecraft formation to the tracked GPS satellites. These slow rotations are caused by the relatively slow orbital motion of high-altitude spacecraft. Slow rates of change of the LOS directions tend to slow the process of resolving double-differenced carrier phase ambiguities as integers.

This study has several goals. The first is to answer the question of whether integer ambiguity resolution is possible in the high-altitude situation of weak signals, high GDOP, and slow LOS rotations. If integer resolution is possible, then additional questions of interest concern the speed of resolution and the resulting accuracy of the relative position solutions. This work is a follow-on to the work reported in Refs. 13 and 14, which study estimation of the relative positions of two user spacecraft using kinematic techniques with L1 signals. The GEO results of Ref. 13 show that ionospheric errors can have a significant impact on accuracy. The present study expands on the work of Refs. 13 and 14 to include dual-frequency measurements in the hope of estimating the ionospheric total electron content (TEC) and removing its effect on the differential position solutions. The challenge in doing this is that integer ambiguities become more difficult to resolve when using dual-frequency carrier phase measurements to estimate and correct for differential TEC [15,16].

References 3-7 and 14 characterize the state of the art of CDGPS for estimation of relative spacecraft positions, and this paper makes two main contributions to this subject area. First, it develops a new relative position estimation algorithm for a pair of Earth-orbiting user receivers. This algorithm resolves double-differenced carrier phase ambiguities for the L1 and L2 signals as integers. The only other estimators that successfully resolve integer ambiguities are reported in Refs. 7 and 14, and only Ref. 7 works with dual-frequency ambiguities. The present work develops an alternative dual-frequency algorithm that is based on kinematic methods. One similarity between the new algorithm and those of Refs. 7 and 14 is its resolution of integers using a least-squares ambiguity decorrelation adjustment (LAMBDA) method and an integer least-squares solver [17,18].

This paper's second contribution is its study of the effectiveness of its ambiguity resolving CDGPS algorithm at high altitudes, i.e., above the GPS constellation. This study is based on a high-fidelity truth-model simulation. It considers cases ranging from GEO to Lunar altitudes.

The remainder of this paper presents its designs, analyses, results, and conclusions in 6 sections. Section II defines the estimator state and presents its models of the measurements and dynamics. Section III describes and explains the new estimation algorithm. Section IV gives a brief overview of the truth-model simulation. Section V presents performance results for the estimator when operating on data from the truth-model simulation. Section VI makes recommendations concerning further improvements to the estimator and further evaluation studies. Section VII gives the paper's conclusions.

II. ESTIMATOR STATE, MEASUREMENT MODELS, AND DYNAMICS MODELS

A. Pseudo-Range Measurement Model and Coarse Pseudo-Range Solution

A standard pseudo-range measurement model has been used to provide a coarse solution for linearization purposes and to provide a soft bound on carrier phase integer ambiguity estimates. The model takes the form [13]:

[*] The problem of weak-signal acquisition and tracking will be greatly alleviated by the new civilian L2 signals that will start to appear soon. The civilian CL signal does not carry data, which allows for longer coherent accumulation intervals and, therefore, higher processing gains that enable the acquisition and tracking of weaker signals [11].

$$P_{1A}^{j} = r_{A}^{j} + c(dt_{RA} - dt^{j}) + TEC_{A}^{j} + n_{P1A}^{j} \quad (1a)$$

$$P_{1B}^{j} = r_{B}^{j} + c(dt_{RB} - dt^{j}) + TEC_{B}^{j} + n_{P1B}^{j} \quad (1b)$$

$$P_{2A}^{j} = r_{A}^{j} + c(dt_{RA} - dt^{j}) + (f_{L1}^{2}/f_{L2}^{2})\, TEC_{A}^{j} + n_{P2A}^{j} \quad (1c)$$

$$P_{2B}^{j} = r_{B}^{j} + c(dt_{RB} - dt^{j}) + (f_{L1}^{2}/f_{L2}^{2})\, TEC_{B}^{j} + n_{P2B}^{j} \quad (1d)$$

where the four P values are pseudo-range measurements. The superscript $()^j$ denotes the signal from GPS satellite j, the 1 or 2 subscript denotes the GPS signal on the L1 or the L2 frequency, and the A or B subscript denotes space-borne user receiver A or B. A similar subscripting and superscripting scheme is used throughout this paper, unless otherwise noted. The distance $r_A^j = [(\boldsymbol{r}_A - \boldsymbol{r}^j)^{\mathrm{T}}(\boldsymbol{r}_A - \boldsymbol{r}^j)]^{0.5}$ is the true range between GPS spacecraft j's location at the time of signal transmission, $\boldsymbol{r}^j$, and user spacecraft A's location at the time of signal reception, $\boldsymbol{r}_A$, and the distance r_B^j is defined similarly for user spacecraft B. The clock errors dt_{RA}, dt_{RB}, and dt^j apply, respectively, to user receivers A and B and to GPS spacecraft j. The quantities TEC_A^j and TEC_B^j are the ionospheric total electron contents along the LOS vectors from user receivers A and B to GPS spacecraft j expressed in equivalent distance units at the L1 frequency. The noise terms n_{P1A}^j, n_{P1B}^j, n_{P2A}^j, and n_{P2B}^j include the effects of receiver thermal noise and multi-path. The parameters f_{L1}, f_{L2}, and c are, respectively, the L1 and L2 carrier frequencies and the speed of light. The geometry associated with these measurements for GPS spacecraft i and j is depicted in Fig. 1.

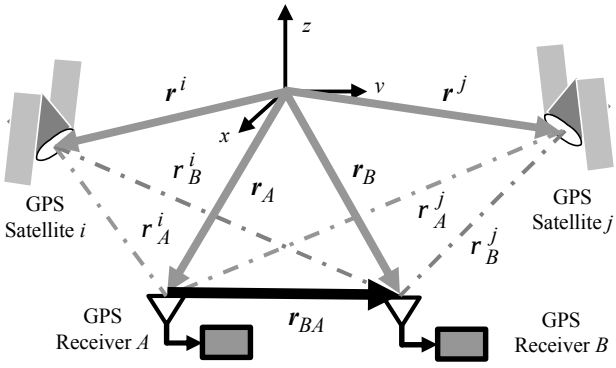

Fig. 1. Geometry of CDGPS measurements for two GPS satellites and two user receivers.

The new estimation algorithm starts by computing the point pseudo-range solutions for the positions, clock errors, and TEC values for user receivers A and B. For receiver A, this procedure involves an iterative nonlinear least-squares solution of eqs. (1a) and (1c) repeated for all $j \in S_A = \{ j_{A1}, ..., j_{An_A} \}$. S_A is the set of indices of the n_A GPS signals that are tracked by receiver A. The solutions that get determined by this procedure are denoted by the $()_{pr}$ subscript; they are $\boldsymbol{r}_{Apr}$, cdt_{RApr}, and $TEC_{Apr}^{j_{A1}}$, ..., $TEC_{Apr}^{j_{An_A}}$. A corresponding solution of eqs. (1b) and (1d) is carried out in order to determine coarse position, clock correction, and TEC values for user receiver B.

B. State Vector of Differential GPS Solution Algorithm

The CDGPS algorithm estimates the following vector of unknowns:

$$\boldsymbol{x}_{tot}(t_k) = \begin{bmatrix} \boldsymbol{x}(t_k) \\ \boldsymbol{T}(t_k) \\ \boldsymbol{e}(t_k) \\ \boldsymbol{a}_{L1} \\ \boldsymbol{a}_{L2} \end{bmatrix} \quad (2)$$

where

$$\boldsymbol{x}(t_k) = \begin{bmatrix} \partial \boldsymbol{r}_A(t_k) \\ \partial \boldsymbol{r}_B(t_k) \\ c\partial dt_{RA}(t_k) \\ c\partial dt_{RB}(t_k) \end{bmatrix} = \begin{bmatrix} \boldsymbol{r}_A(t_k) - \boldsymbol{r}_{Apr}(t_k) \\ \boldsymbol{r}_B(t_k) - \boldsymbol{r}_{Bpr}(t_k) \\ c\{dt_{RA}(t_k) - dt_{RApr}(t_k)\} \\ c\{dt_{RB}(t_k) - dt_{RBpr}(t_k)\} \end{bmatrix} \quad (3a)$$

$$\boldsymbol{T}(t_k) = \begin{bmatrix} \partial TEC_A^{j_{A1}}(t_k) \\ \vdots \\ \partial TEC_A^{j_{An_A}}(t_k) \\ \partial TEC_B^{j_{B1}}(t_k) \\ \vdots \\ \partial TEC_B^{j_{Bn_B}}(t_k) \end{bmatrix} = \begin{bmatrix} TEC_A^{j_{A1}}(t_k) - TEC_{Apr}^{j_{A1}}(t_k) \\ \vdots \\ TEC_A^{j_{An_A}}(t_k) - TEC_{Apr}^{j_{An_A}}(t_k) \\ TEC_B^{j_{B1}}(t_k) - TEC_{Bpr}^{j_{B1}}(t_k) \\ \vdots \\ TEC_B^{j_{Bn_B}}(t_k) - TEC_{Bpr}^{j_{Bn_B}}(t_k) \end{bmatrix} \quad (3b)$$

$$\boldsymbol{e}(t_k) = \begin{bmatrix} \partial \boldsymbol{r}^1(t_k) \\ c\partial dt^1(t_k) \\ \vdots \\ \partial \boldsymbol{r}^n(t_k) \\ c\partial dt^n(t_k) \end{bmatrix} \quad (3c)$$

$$\boldsymbol{a}_{L1} = \begin{bmatrix} a_{1A}^{j_{A1}} \\ \vdots \\ a_{1A}^{j_{An_A}} \\ a_{1B}^{j_{B1}} \\ \vdots \\ a_{1B}^{j_{Bn_B}} \end{bmatrix} \text{ and } \boldsymbol{a}_{L2} = \begin{bmatrix} a_{2A}^{j_{A1}} \\ \vdots \\ a_{2A}^{j_{An_A}} \\ a_{2B}^{j_{B1}} \\ \vdots \\ a_{2B}^{j_{Bn_B}} \end{bmatrix} \quad (3d)$$

The vectors $\boldsymbol{x}(t_k)$, $\boldsymbol{T}(t_k)$, and $\boldsymbol{e}(t_k)$ apply at sample time t_k, and they can vary with time. Each of these vectors consists of perturbations, as denoted by the ∂ prefix. The 8-dimensional vector $\boldsymbol{x}(t_k)$ consists of the perturbations of the true positions and the true range-equivalent clock corrections for receivers A and B from their pseudo-range-based solutions. The position perturbations are given in Earth-centered inertial coordinates (ECIF). The (n_A+n_B)-dimensional vector $\boldsymbol{T}(t_k)$ consists of the perturbations of true TEC values from their pseudo-range-based estimates. These values correspond to integrated electron densities along LOS vectors from receiver A to n_A GPS satellites and from receiver B to n_B GPS satellites. The CDGPS-

based estimates of the perturbation in $\boldsymbol{x}(t_k)$ and $\boldsymbol{T}(t_k)$ are added to the corresponding pseudo-range-based estimates in order to compute these quantities' absolute CDGPS estimates. The $4n$-dimensional vector $\boldsymbol{e}(t_k)$ contains the ECIF position perturbation vectors $\partial \boldsymbol{r}^j(t_k)$ and the range-equivalent clock perturbations $c\partial dt^j(t_k)$ for GPS satellites j = 1, ..., n. These quantities are corrections to the position vectors and transmitter clock errors as determined from the broadcast ephemerides of each GPS spacecraft.

The (n_A+n_B)-dimensional vectors $\boldsymbol{a}_{L1}$ and $\boldsymbol{a}_{L2}$ contain the ambiguities for the L1 and L2 carrier phase measurements, respectively. The $\boldsymbol{a}_{L1}$ components a^i_{1A} and a^j_{1B} are the L1 carrier phase ambiguities of, respectively, GPS satellite i as tracked by receiver A and GPS satellite j as tracked by receiver B. The $\boldsymbol{a}_{L2}$ components a^i_{2A} and a^j_{2B} are similar, except that they are L2 carrier phase ambiguities. These quantities are usually denoted by N rather than a. The current designation is used in order to emphasize the fact that these quantities are not necessarily integers [13]. These ambiguities should be constants [13], and the estimator treats them as such.

The estimator keeps track of un-differenced carrier phase ambiguities, but it computes its state estimate in a way which ensures that double-differences of these quantities take on integer values. This approach differs from typical CDGPS practice in which single- or double-differenced ambiguities are direct states of the estimator. There are two reasons for using the present unconventional formulation. First, it explicitly recognizes the fact that these ambiguities are constants. This allows it to derive additional information from them. Estimators that keep track of differenced ambiguities implicitly assume that each un-differenced ambiguity contains a time-varying real component. Their differencing operations can be viewed as point-wise estimation of each time-varying, real-valued component followed by removal of it. If the real-valued components are constants, then differencing operations implicitly discard information by ignoring their constancy.

The new estimator will achieve improved results through the retention of un-differenced ambiguities only if the constancy assumption is true. The primary causes of non-constancy are TEC variations and inaccuracies in the broadcast GPS navigation data. The explicit estimation of $\boldsymbol{T}(t_k)$ and $\boldsymbol{e}(t_k)$ provides a means of assuring that the ambiguities are constants.

Two additional advantages accrue from using un-differenced ambiguities. First, there is no cross correlation in the initial measurement equations, which are also un-differenced. This allows a simpler formulation of the optimal estimation problem. Second, carrier cycle slips become easier to identify and correct. Note, however, that the issue of cycle slips is not addressed in the present work.

C. Linearized Pseudo-Range and Carrier Phase Measurement Models

The CDGPS algorithm uses pseudo-range and carrier phase measurement models that have been linearized about the pseudo-range solutions. The linearized pseudo-range models are linearizations of eqs. (1a)-(1d) and take the form:

$$\begin{aligned} P^j_{1A} - r^j_{Apr} - c(dt_{RApr} - dt^j) - TEC^j_{Apr} \;=\; & \\ (\hat{r}^j_A)^{\mathrm{T}}(\partial \boldsymbol{r}_A - \partial \boldsymbol{r}^j) + c(\partial dt_{RA} - \partial dt^j) & \\ + \partial TEC^j_A + n^j_{P1A} & \end{aligned} \tag{4a}$$

$$\begin{aligned} P^j_{1B} - r^j_{Bpr} - c(dt_{RBpr} - dt^j) - TEC^j_{Bpr} \;=\; & \\ (\hat{r}^j_B)^{\mathrm{T}}(\partial \boldsymbol{r}_B - \partial \boldsymbol{r}^j) + c(\partial dt_{RB} - \partial dt^j) & \\ + \partial TEC^j_B + n^j_{P1B} & \end{aligned} \tag{4b}$$

$$\begin{aligned} P^j_{2A} - r^j_{Apr} - c(dt_{RApr} - dt^j) - (f^2_{L1}/f^2_{L2})TEC^j_{Apr} \;=\; & \\ (\hat{r}^j_A)^{\mathrm{T}}(\partial \boldsymbol{r}_A - \partial \boldsymbol{r}^j) + c(\partial dt_{RA} - \partial dt^j) & \\ + (f^2_{L1}/f^2_{L2})\partial TEC^j_A + n^j_{P2A} & \end{aligned} \tag{4c}$$

$$\begin{aligned} P^j_{2B} - r^j_{Bpr} - c(dt_{RBpr} - dt^j) - (f^2_{L1}/f^2_{L2})TEC^j_{Bpr} \;=\; & \\ (\hat{r}^j_B)^{\mathrm{T}}(\partial \boldsymbol{r}_B - \partial \boldsymbol{r}^j) + c(\partial dt_{RB} - \partial dt^j) & \\ + (f^2_{L1}/f^2_{L2})\partial TEC^j_B + n^j_{P2B} & \end{aligned} \tag{4d}$$

where $\hat{r}^j_A$ and $\hat{r}^j_B$ are the unit vectors that point from the transmission-time locations of GPS spacecraft j to the pseudo-range positions of receivers A and B. Most of the quantities in eqs. (4a)-(4d) are functions of the sample time, t_k. In the interest of saving space, this dependence has not been explicitly noted.

The following are linearized measurement models for the L1 and L2 beat carrier phases that are output by receivers A and B:

$$\begin{aligned} l_{L1}f^j_{1A} - r^j_{Apr} - c(dt_{RApr} - dt^j) + TEC^j_{Apr} \;=\; & \\ (\hat{r}^j_A)^{\mathrm{T}}(\partial \boldsymbol{r}_A - \partial \boldsymbol{r}^j) + c(\partial dt_{RA} - \partial dt^j) & \\ - \partial TEC^j_A + l_{L1}a^j_{1A} + l_{L1}n^j_{f1A} & \end{aligned} \tag{5a}$$

$$\begin{aligned} l_{L1}f^j_{1B} - r^j_{Bpr} - c(dt_{RBpr} - dt^j) + TEC^j_{Bpr} \;=\; & \\ (\hat{r}^j_B)^{\mathrm{T}}(\partial \boldsymbol{r}_B - \partial \boldsymbol{r}^j) + c(\partial dt_{RB} - \partial dt^j) & \\ - \partial TEC^j_B + l_{L1}a^j_{1B} + l_{L1}n^j_{f1B} & \end{aligned} \tag{5b}$$

$$\begin{aligned} l_{L2}f^j_{2A} - r^j_{Apr} - c(dt_{RApr} - dt^j) + (f^2_{L1}/f^2_{L2})TEC^j_{Apr} \;=\; & \\ (\hat{r}^j_A)^{\mathrm{T}}(\partial \boldsymbol{r}_A - \partial \boldsymbol{r}^j) + c(\partial dt_{RA} - \partial dt^j) & \end{aligned}$$

$$-(f_{L1}^2/f_{L2}^2)\partial TEC_A^j + l_{L2}a_{2A}^j + l_{L2}n_{f2A}^j \quad (5c)$$

$$l_{L2}f_{2B}^j - r_{Bpr}^j - c(dt_{RBpr} - dt^j) + (f_{L1}^2/f_{L2}^2)TEC_{Bpr}^j = (\hat{r}_B^j)^{\mathrm{T}}(\partial \boldsymbol{r}_B - \partial \boldsymbol{r}^j) + c(\partial dt_{RB} - \partial dt^j) - (f_{L1}^2/f_{L2}^2)\partial TEC_B^j + l_{L2}a_{2B}^j + l_{L2}n_{f2B}^j \quad (5d)$$

where the quantities f_{1A}^j, f_{1B}^j, f_{2A}^j, and f_{2B}^j are the actual beat carrier phase measurements given in cycles. The parameters l_{L1} (=c/f_{L1}) and l_{L2} (=c/f_{L2}) are the standard nominal carrier wavelengths of the L1 and L2 signals, respectively. The terms n_{f1A}^j, n_{f1B}^j, n_{f2A}^j, and n_{f2B}^j represent carrier phase measurement errors due to multi-path, carrier phase wind-up, and receiver thermal noise [13]. The standard deviations of these noise terms are usually on the order of (0.01m)/l or less, which is why CDGPS techniques can be very accurate. Note how eqs. (5a)-(5d) resemble eqs. (4a)-(4d), except for the reversals of sign in the TEC terms and the additional ambiguity biases $l_{L1}a_{1A}^j$, $l_{L1}a_{1B}^j$, $l_{L2}a_{2A}^j$, and $l_{L2}a_{2B}^j$.

The models in eqs. (5a)-(5b) are linearizations of the carrier phase model given in Ref. 13, which has been derived from first principles in order to better understand the nature of the ambiguity bias terms. The present models vary from that of Ref. 13 because they recognize that the nominal transmitter clock correction can be lumped into a single term on the left-hand side of each equation.

D. Pseudo-Measurement of the Single-Differenced TEC

The discussions of Refs. 15 and 16 indicate that it is difficult to resolve double-differenced carrier phase ambiguities as exact integers when using dual frequency measurements to determine both relative position and double-differenced TEC. In order to understand this difficulty, consider the TEC-free equivalent L1 carrier phase measurement for receiver A:

$$l_{L1}\left[\frac{f_{L1}(f_{L1}f_{1A}^j - f_{L2}f_{2A}^j)}{f_{L1}^2 - f_{L2}^2}\right] = r_A^j + c(dt_{RA} - dt^j) + l_{L1}\left[\frac{f_{L1}(f_{L1}a_{1A}^j - f_{L2}a_{2A}^j)}{f_{L1}^2 - f_{L2}^2}\right] + l_{L1}\left[\frac{f_{L1}(f_{L1}n_{f1A}^j - f_{L2}n_{f2A}^j)}{f_{L1}^2 - f_{L2}^2}\right] \quad (6)$$

This measurement uses the difference of the range-equivalent L2 and L1 carrier-phase measurements to solve for TEC_A^j. This solution is then substituted back into the L1 equation. The ratio f_{L1}/f_{L2} = 77/60 can be used to define the transformed ambiguity pair $\tilde{a}_{1A}^j = 77a_{1A}^j - 60a_{2A}^j$ and $\tilde{a}_{2A}^j = -9a_{1A}^j + 7a_{2A}^j$. The inverse transformations are $a_{1A}^j = -7\tilde{a}_{1A}^j - 60\tilde{a}_{2A}^j$ and $a_{2A}^j = -9\tilde{a}_{1A}^j - 77\tilde{a}_{2A}^j$. The transformed ambiguities preserve the integer nature of their double-differences because there is a one-to-one mapping between integer values of $[a_{1A}^j; a_{2A}^j]$ and integer values of $[\tilde{a}_{1A}^j; \tilde{a}_{2A}^j]$. The TEC-free equivalent L1 carrier phase measurement model can be re-written using the new $\tilde{a}_{1A}^j$ ambiguity:

$$l_{L1}\left[\frac{f_{L1}(f_{L1}f_{1A}^j - f_{L2}f_{2A}^j)}{f_{L1}^2 - f_{L2}^2}\right] = r_A^j + c(dt_{RA} - dt^j) + l_{L1}\left[\frac{f_{L1}^2}{77(f_{L1}^2 - f_{L2}^2)}\right]\tilde{a}_{1A}^j + l_{L1}\left[\frac{f_{L1}(f_{L1}n_{f1A}^j - f_{L2}n_{f2A}^j)}{f_{L1}^2 - f_{L2}^2}\right] \quad (7)$$

The form of eq. (7) causes two problems when trying to resolve integer ambiguities. First, the effective wavelength of the ambiguity is reduced to $l_{L1}f_{L1}^2/[77(f_{L1}^2 - f_{L2}^2)]$ = 0.0063 m. Second, the equivalent standard deviation of the final noise term is increased by a factor of 3.2 compared to the original L1 carrier phase noise, which makes the typical noise standard deviation larger than 0.01 m. Resolution of the ambiguities as integers is very difficult when the noise standard deviation is larger than the ambiguity wavelength.

The estimator combats this ambiguity problem by adding a pseudo-measurement of the single-differenced TEC. The linearized model for this pseudo-measurement is:

$$TEC_{Apr}^j - TEC_{Bpr}^j = -\partial TEC_A^j + \partial TEC_B^j + n_{DTEC}^j \quad (8)$$

where n_{DTEC}^j is a pseudo-noise term. Its modeled standard deviation, s_{DTEC}^j, gives a measure of the expected magnitude of the difference between TEC_A^j and TEC_B^j. This standard deviation is a tuning parameter of the estimator. A large s_{DTEC}^j value indicates little or no correlation between the TEC values along the LOS vectors from the two user receivers to GPS satellite j. In this case, the estimator will have the same difficulty in resolving integer ambiguities that it would have had if it had used the TEC-free carrier phase measurement in eq. (7). A small value of s_{DTEC}^j will tell the estimator that it can use single-differences between receivers in order to remove most of the TEC effects from the L1 and L2 measurements. An intermediate value of s_{DTEC}^j allows the estimator to determine TEC_A^j and TEC_B^j using the L1 and L2 carrier phase and pseudo-range measurements, but it limits the number of possible ambiguities to those that produce reasonable TEC single differences. Reasonable limits can be achieved for relatively large values of s_{DTEC}^j because a unit change in $\tilde{a}_{1A}^j$ causes the L1/L2

carrier-phase-based estimate of TEC_A^j to change by 8.2 TEC units, which is a large change.

This approach is similar to the ionosphere-weighted approach of Ref. 15. The main difference is that the current approach does not use *a priori* information about the ionosphere other than an estimate of s_{DTEC}^j. The method of Ref. 15 also uses an *a priori* double-differenced TEC value. It is likely that the Ref. 15 estimator can use a lower equivalent s_{DTEC}^j to model the residual errors, but its need for an *a priori* estimate of the double-differenced TEC represents a level of complication that the present formulation seeks to avoid.

E. Dynamics Models

The estimator uses limited dynamics models that are appropriate to its kinematic approach to CDGPS estimation. The receiver position and clock error states in $\boldsymbol{x}(t_k)$ and the ionospheric TEC states in $\boldsymbol{T}(t_k)$ are modeled as being uncorrelated in time. That is, there is no dynamic relationship used between $\boldsymbol{x}(t_k)$ and $\boldsymbol{x}(t_{k-1})$ or between $\boldsymbol{T}(t_k)$ and $\boldsymbol{T}(t_{k-1})$. Therefore, these quantities must be re-estimated from scratch at each measurement sample based purely on the measurement data from that sample, which is consistent with the kinematic approach.

The states associated with the GPS satellites' residual position and clock corrections are modeled as evolving according to a first-order Gauss-Markov process:

$$\boldsymbol{e}(t_k) = a_{k-1}\boldsymbol{e}(t_{k-1}) + b_{k-1}\boldsymbol{w}_{e(k-1)} \tag{9}$$

where $a_{k-1} = exp[(t_k - t_{k-1})/t\,]$ and $b_{k-1} = s_e[1 - exp\{2(t_k - t_{k-1})/t\,\}]^{0.5}$ are scalars and where $\boldsymbol{w}_{e(k-1)}$ is a Gaussian discrete-time white-process-noise vector whose mean is zero and whose covariance equals the identity matrix. The scalar t is the correlation time of the Markov process, and the scalar s_e is the steady-state standard deviation of each of its $4n$ independent components.

The real-valued, un-differenced ambiguity vectors $\boldsymbol{a}_{L1}$ and $\boldsymbol{a}_{L2}$ are modeled as being constant. Their dynamic models take the forms $\boldsymbol{a}_{L1(k)} = \boldsymbol{a}_{L1(k-1)} = \boldsymbol{a}_{L1}$ and $\boldsymbol{a}_{L2(k)} = \boldsymbol{a}_{L2(k-1)} = \boldsymbol{a}_{L2}$. These models could be augmented to include the possibility of cycle slips, but that would introduce the need for hypothesis testing in order to implement a cycle slip recovery procedure, as in Ref. 14. The design of such an algorithm is beyond the scope of the present paper.

III. ESTIMATION ALGORITHM

A. Square-Root Information Format

The estimation algorithm uses Square-Root Information Filter (SRIF) methods [19] to propagate, update, and store its estimates and covariances for the components of the $\boldsymbol{x}_{tot}(t_k)$ vector. The SRIF format uses a square-root information equation of the form $R\boldsymbol{x} = \boldsymbol{z} - n$ in order to keep track of its mean and covariance for $\boldsymbol{x}$. The square, nonsingular matrix R and the vector $\boldsymbol{z}$ are computed by the estimator, and the Gaussian noise vector n is modeled as having a mean of zero and a covariance equal to the identity matrix. These facts imply that the estimate and its error covariance are, respectively, $\hat{\boldsymbol{x}} = R^{-1}\boldsymbol{z}$ and $P_{xx} = R^{-1}(R^{-1})^{\mathrm{T}}$. Note that all subsequently defined n vectors in this paper are assumed to be Gaussian white-noise vectors with means equal to zero, covariances equal to the identity matrix, and zero cross-correlation with all other noise vectors.

The SRIF uses a measurement equation of the form:

$$\begin{aligned}\boldsymbol{y}(t_k) = {} & H_{x(k)}\boldsymbol{x}(t_k) + H_{T(k)}\boldsymbol{T}(t_k) + H_{e(k)}\boldsymbol{e}(t_k) \\ & + H_{a1(k)}\boldsymbol{a}_{L1(k)} + H_{a2(k)}\boldsymbol{a}_{L2(k)} + n_{yk}\end{aligned} \tag{10}$$

where the measurement vector $\boldsymbol{y}(t_k)$ and the matrices $H_{x(k)}$, $H_{T(k)}$, $H_{e(k)}$, $H_{a1(k)}$, and $H_{a2(k)}$ are known. This vector equation includes all of the linearized measurement models in eqs. (4a)-(5d) and (8) for all of the tracked GPS satellites. Each such equation is divided by the modeled standard deviation of its measurement error in order to be in the correct format for inclusion as a component of eq. (10). The resulting equations are used to determine $\boldsymbol{y}(t_k)$, $H_{x(k)}$, $H_{T(k)}$, $H_{e(k)}$, $H_{a1(k)}$, and $H_{a2(k)}$.

The estimator must keep track of the GPS satellites for which eq. (10) models pseudo-range and carrier phase measurements and single-differenced TEC pseudo-measurements. $S_{A(k)}$ is the set of satellite identifier numbers (SVIDs) of the GPS spacecraft for which receiver A returns pseudo-range and carrier phase data at sample time t_k. It contains $n_{A(k)}$ elements. Similarly, the set $S_{B(k)}$ contains the SVIDs of the $n_{B(k)}$ GPS spacecraft whose pseudo-range and carrier phase data are returned by receiver B at sample time t_k. The set $S_{com(k)} = S_{A(k)} \cap S_{B(k)}$ contains the two sets' common SVIDs, which number $n_{com(k)} \le \min[n_{A(k)}, n_{B(k)}]$. The dimension of $\boldsymbol{y}(t_k)$ is $4[n_{A(k)} + n_{B(k)}] + n_{com(k)}$ because each receiver returns both L1 and L2 pseudo-range and carrier phase for each tracked satellite and because there is a single-differenced TEC pseudo-measurement for each satellite that is visible to both receivers.

B. A Priori Information

The estimator uses *a priori* information about the GPS position and clock errors and about the carrier phase ambiguities. The *a priori* information used at sample time t_k consists of all of the relevant information that has been amassed from all of the preceding sample times. This information is stored in the following square-root format:

$$\begin{bmatrix} R_{ee(k-1)} & R_{ea(k-1)} \\ 0 & R_{aa(k-1)} \end{bmatrix} \begin{bmatrix} \boldsymbol{e}(t_{k-1}) \\ \boldsymbol{a}_{L1(k-1)} \\ \boldsymbol{a}_{L2(k-1)} \end{bmatrix} = \begin{bmatrix} \boldsymbol{z}_{e(k-1)} \\ \boldsymbol{z}_{a(k-1)} \end{bmatrix} - \begin{bmatrix} n_{e(k-1)} \\ n_{a(k-1)} \end{bmatrix} \tag{11}$$

The matrices $R_{ee(k-1)}$ and $R_{aa(k-1)}$ are square, upper-triangular, and non-singular with dimensions $4n$-by-$4n$ and $2[n_{A(k-1)}+n_{B(k-1)}]$-by-$2[n_{A(k-1)}+n_{B(k-1)}]$, respectively. The matrix $R_{ea(k-1)}$ has dimension $4n$-by-$2[n_{A(k-1)}+n_{B(k-1)}]$. The vector $\boldsymbol{z}_{e(k-1)}$ has dimension $4n$, and the vector $\boldsymbol{z}_{a(k-1)}$ has dimension $2[n_{A(k-1)}+n_{B(k-1)}]$. The matrices $R_{ee(k-1)}$, $R_{ea(k-1)}$, and $R_{aa(k-1)}$ and the vectors $\boldsymbol{z}_{e(k-1)}$ and $\boldsymbol{z}_{a(k-1)}$ are computed by the estimator.

The possibility of a change of tracked satellites from sample time t_{k-1} to sample time t_k necessitates the use of the notation $\boldsymbol{a}_{L1(k-1)}$ and $\boldsymbol{a}_{L2(k-1)}$ to distinguish the un-differenced ambiguity vectors associated with different sample times. Although the carrier phase ambiguity for a given tracked satellite/receiver pair does not change, the vectors $\boldsymbol{a}_{L1(k-1)}$ and $\boldsymbol{a}_{L2(k-1)}$ will change if the elements of the set $S_{A(k-1)}$ or the set $S_{B(k-1)}$ change. This happens because $\boldsymbol{a}_{L1(k-1)}$ and $\boldsymbol{a}_{L2(k-1)}$ only store the ambiguities associated with the tracked GPS satellites in $S_{A(k-1)}$ and $S_{B(k-1)}$.

If the first measurement sample occurs at sample t_0, then the estimator must initialize its *a priori* information at fictitious sample time $t_{-1} < t_0$. It initializes $R_{ee(-1)}$ to equal the $4n$-by-$4n$ identity matrix multiplied by $1/s_e$, and it sets $\boldsymbol{z}_{e(-1)} = 0$. There are no tracked satellites prior to time t_0; therefore, the index sets $S_{A(-1)}$ and $S_{B(-1)}$ are set equal to the empty set. This implies that $\boldsymbol{a}_{L1(-1)}$, $\boldsymbol{a}_{L2(-1)}$, and $\boldsymbol{z}_{a(-1)}$ are empty vectors and that $R_{ea(-1)}$ and $R_{aa(-1)}$ are empty matrices.

C. Dynamic Propagation and Measurement Update

The SRIF calculations involve the usual Kalman filter dynamic propagation followed by a measurement update. The dynamic propagation maps the *a priori* information in eq. (11) forwards to time t_k using the dynamic models of Section II.E. The measurement update combines the propagated *a priori* information with the new measurement information in eq. (10).

Dynamic Propagation. The dynamic propagation starts with a propagation of the GPS position/transmitter-clock error vector $\boldsymbol{e}$. These propagation calculations could use the traditional SRIF methods of Ref. 19, but an alternate method is chosen that works even when a_{k-1} of eq. (9) is zero. This alternate method is based on singular SRIF principles like those used in Ref. 20. The method starts by using orthonormal/upper-triangular (QR) factorization [21] to compute

$$Q_{1(k)}\begin{bmatrix}\widetilde{R}_{ww(k)} & \widetilde{R}_{we(k)}\\ 0 & \widetilde{R}_{ee(k)}\end{bmatrix} = \frac{1}{a_{k-1}^2+b_{k-1}^2}\begin{bmatrix}-a_{k-1}I & b_{k-1}I\\ b_{k-1}R_{ee(k-1)} & a_{k-1}R_{ee(k-1)}\end{bmatrix} \quad (12)$$

$Q_{1(k)}$ is an orthonormal matrix, i.e., $Q_{1(k)}Q_{1(k)}^{\mathrm{T}} = I$. $\widetilde{R}_{ww(k)}$ and $\widetilde{R}_{ee(k)}$ are square, upper-triangular, non-singular matrixes of dimension $4n$-by-$4n$, and $\widetilde{R}_{we(k)}$ is another matrix of the same dimension. The orthonormal matrix is then used to compute the matrix $\breve{R}_{ea(k-1)}$ and the vector $\widetilde{z}_{e(k)}$ according to the formulas

$$\breve{R}_{ea(k-1)} = [0\ I]Q_{1(k)}^{\mathrm{T}}\begin{bmatrix}0\\ R_{ea(k-1)}\end{bmatrix} \text{ and}$$

$$\widetilde{z}_{e(k)} = [0\ I]Q_{1(k)}^{\mathrm{T}}\begin{bmatrix}0\\ z_{e(k-1)}\end{bmatrix} \quad (13)$$

These operations result in an *a priori* square-root information equation that takes the form:

$$\begin{bmatrix}\widetilde{R}_{ee(k)} & \breve{R}_{ea(k-1)}\\ 0 & R_{aa(k-1)}\end{bmatrix}\begin{bmatrix}\boldsymbol{e}(t_k)\\ \begin{bmatrix}\boldsymbol{a}_{L1(k-1)}\\ \boldsymbol{a}_{L2(k-1)}\end{bmatrix}\end{bmatrix} = \begin{bmatrix}\widetilde{z}_{e(k)}\\ z_{a(k-1)}\end{bmatrix} - \begin{bmatrix}\widetilde{n}_{e(k)}\\ n_{a(k-1)}\end{bmatrix} \quad (14)$$

The remaining dynamic propagation operations account for the changes in tracked satellites, which are reflected in differences between the old tracking index sets $S_{A(k-1)}$ and $S_{B(k-1)}$ and the new index sets $S_{A(k)}$ and $S_{B(k)}$. These index sets can be used to construct matrices $U_{D(k-1)}$, $U_{K(k-1)}$, and $V_{(k)}$ that have the following properties: Each row of $U_{D(k-1)}$ and $U_{K(k-1)}$ is a 1-by-$[n_{A(k-1)}+n_{B(k-1)}]$ row vector with all zero entries except for one entry that equals 1, and each row of $V_{(k)}$ is similar, except that its dimension is 1-by-$[n_{A(k)}+n_{B(k)}]$. The $[n_{A(k-1)}+n_{B(k-1)}]$-by-$[n_{A(k-1)}+n_{B(k-1)}]$ matrix $U_{(k-1)} = [U_{D(k-1)};U_{K(k-1)}]$ is a permutation matrix. The vectors $\boldsymbol{a}_{DL1(k-1)} = U_{D(k-1)}\boldsymbol{a}_{L1(k-1)}$ and $\boldsymbol{a}_{DL2(k-1)} = U_{D(k-1)}\boldsymbol{a}_{L2(k-1)}$ contain all of the carrier phase ambiguities for the GPS satellites that are tracked at sample time t_{k-1} but not at sample time t_k. These are the ambiguities that must get discarded before the measurement update at time t_k. The vectors $U_{K(k-1)}\boldsymbol{a}_{L1(k-1)} = V_{(k)}\boldsymbol{a}_{L1(k)}$ and $U_{K(k-1)}\boldsymbol{a}_{L2(k-1)} = V_{(k)}\boldsymbol{a}_{L2(k)}$ contain all of the ambiguities that are tracked at both sample times and therefore retained at sample time t_k. The construction of these matrices amounts to an accounting calculation that involves comparisons of the indices in $S_{A(k-1)}$ and $S_{B(k-1)}$ with the indices in $S_{A(k)}$ and $S_{B(k)}$ along with mappings of those indices to the corresponding entries in $\boldsymbol{a}_{L1(k-1)}$, $\boldsymbol{a}_{L2(k-1)}$, $\boldsymbol{a}_{L1(k)}$, and $\boldsymbol{a}_{L2(k)}$. This analysis assumes that common index mappings are used for the pair $\boldsymbol{a}_{L1(k-1)}$ and $\boldsymbol{a}_{L2(k-1)}$ and for the pair $\boldsymbol{a}_{L1(k)}$ and $\boldsymbol{a}_{L2(k)}$.

A transformation and a QR factorization are required in order to delete the old ambiguities in $\boldsymbol{a}_{DL1(k-1)}$ and $\boldsymbol{a}_{DL2(k-1)}$ while mapping the information for the ambiguities in $U_{K(k-1)}\boldsymbol{a}_{L1(k-1)}$ and $U_{K(k-1)}\boldsymbol{a}_{L2(k-1)}$ into the correct locations for use with the new ambiguity vectors $\boldsymbol{a}_{L1(k)}$ and $\boldsymbol{a}_{L2(k)}$. The transformation takes the form:

$$\begin{bmatrix}\widetilde{R}_{eD(k)} & \widetilde{R}_{ea(k)}\\ \widetilde{R}_{aD(k)} & \widetilde{R}_{aa(k)}\end{bmatrix} = \begin{bmatrix}\breve{R}_{ea(k-1)}\\ R_{aa(k-1)}\end{bmatrix}\begin{bmatrix}U_{(k-1)}^{\mathrm{T}} & 0\\ 0 & U_{(k-1)}^{\mathrm{T}}\end{bmatrix}\begin{bmatrix}I & 0 & 0 & 0\\ 0 & 0 & V_{(k)} & 0\\ 0 & I & 0 & 0\\ 0 & 0 & 0 & V_{(k)}\end{bmatrix} \quad (15)$$

The ambiguity propagation finishes by performing the

following QR factorization

$$Q_{2(k)}\begin{bmatrix} \bar{R}_{DD(k)} & \bar{R}_{De(k)} & \bar{R}_{Da(k)} \\ 0 & \bar{R}_{ee(k)} & \bar{R}_{ea(k)} \\ 0 & 0 & \bar{R}_{aa(k)} \end{bmatrix} = \begin{bmatrix} \tilde{R}_{eD(k)} & \tilde{R}_{ee(k)} & \tilde{R}_{ea(k)} \\ \tilde{R}_{aD(k)} & 0 & \tilde{R}_{aa(k)} \end{bmatrix} \tag{16}$$

followed by the vector transformation

$$\begin{bmatrix} \bar{z}_{D(k)} \\ \bar{z}_{e(k)} \\ \bar{z}_{a(k)} \end{bmatrix} = Q_{2(k)}^{\mathrm{T}} \begin{bmatrix} \tilde{z}_{e(k)} \\ z_{a(k-1)} \end{bmatrix} \tag{17}$$

The matrix $Q_{2(k)}$ is orthonormal, and the matrices $\bar{R}_{DD(k)}$ and $\bar{R}_{ee(k)}$ are square, upper-triangular, and non-singular. The matrix $\bar{R}_{aa(k)}$ is upper-triangular, but it will have more columns than rows if new tracked satellites appear in either of the index sets $S_{A(k)}$ or $S_{B(k)}$. The matrices $\bar{R}_{DD(k)}$, $\bar{R}_{De(k)}$, and $\bar{R}_{Da(k)}$ and the vector $\bar{z}_{D(k)}$ are associated with an information equation for the dropped ambiguity vector $[\boldsymbol{a}_{DL1(k\text{-}1)};\boldsymbol{a}_{DL2(k\text{-}1)}]$. Therefore, they can be discarded. The matrices $\bar{R}_{ee(k)}$, $\bar{R}_{ea(k)}$, and $\bar{R}_{aa(k)}$ and the vectors $\bar{z}_{e(k)}$ and $\bar{z}_{a(k)}$ constitute the *a priori* information for the unknown vectors $\boldsymbol{e}(t_k)$ and $[\boldsymbol{a}_{L1(k)};\boldsymbol{a}_{L2(k)}]$.

The discarding of information about the ambiguity vector $[\boldsymbol{a}_{DL1(k\text{-}1)};\boldsymbol{a}_{DL2(k\text{-}1)}]$ is sub-optimal when integer ambiguities are used. It is possible that some of these un-differenced, real-valued ambiguities are used to form double-differences whose integer values have been correctly identified. Wholesale discarding of the information in $\bar{R}_{DD(k)}$, $\bar{R}_{De(k)}$, $\bar{R}_{Da(k)}$, and $\bar{z}_{D(k)}$ involves a loss of knowledge about the values of any such double-differenced ambiguities. The development of optimal means to retain this information in the context of SRIF calculations is beyond the scope of this paper.

Measurement Update. The measurement update uses standard SRIF calculations in order to combine the *a priori* information in the last two lines of eqs. (16) and (17) with the information in measurement eq. (10). These calculations start with the QR factorization

$$Q_{3(k)}\begin{bmatrix} R_{xx(k)} & R_{xT(k)} & R_{xe(k)} & R_{xa(k)} \\ 0 & R_{TT(k)} & R_{Te(k)} & R_{Ta(k)} \\ 0 & 0 & R_{ee(k)} & R_{ea(k)} \\ 0 & 0 & 0 & R_{aa(k)} \\ 0 & 0 & 0 & 0 \end{bmatrix} = \begin{bmatrix} H_{x(k)} & H_{T(k)} & H_{e(k)} & [H_{a1(k)}\ H_{a2(k)}] \\ 0 & 0 & \bar{R}_{ee(k)} & \bar{R}_{ea(k)} \\ 0 & 0 & 0 & \bar{R}_{aa(k)} \end{bmatrix} \tag{18}$$

and finish with the vector transformation

$$\begin{bmatrix} z_{x(k)} \\ z_{T(k)} \\ z_{e(k)} \\ z_{a(k)} \\ z_{r(k)} \end{bmatrix} = Q_{3(k)}^{\mathrm{T}} \begin{bmatrix} \boldsymbol{y}(t_k) \\ \bar{z}_{e(k)} \\ \bar{z}_{a(k)} \end{bmatrix} \tag{19}$$

The matrix $Q_{3(k)}$ is orthonormal, and the matrices $R_{xx(k)}$, $R_{TT(k)}$, $R_{ee(k)}$, and $R_{aa(k)}$ are square, upper-triangular, and non-singular. The number of rows and columns in each of these matrices equals the number of rows in the corresponding estimated vector, $\boldsymbol{x}(t_k)$, $\boldsymbol{T}(t_k)$, $\boldsymbol{e}(t_k)$, or $[\boldsymbol{a}_{L1(k)};\boldsymbol{a}_{L2(k)}]$. The matrices $R_{xT(k)}$, $R_{xe(k)}$, $R_{xa(k)}$, $R_{Te(k)}$, $R_{Ta(k)}$, and $R_{ea(k)}$ and the information vectors $z_{x(k)}$, $z_{T(k)}$, $z_{e(k)}$, and $z_{a(k)}$ all have appropriate dimensions. The vector $z_{r(k)}$ contains the residual errors of the optimal estimate that uses only real-valued ambiguities.

The information matrices and vectors in eqs. (18) and (19) can be used to form the following *a posteriori* square-root information equation

$$\begin{bmatrix} R_{xx(k)} & R_{xT(k)} & R_{xe(k)} & R_{xa(k)} \\ 0 & R_{TT(k)} & R_{Te(k)} & R_{Ta(k)} \\ 0 & 0 & R_{ee(k)} & R_{ea(k)} \\ 0 & 0 & 0 & R_{aa(k)} \end{bmatrix} \begin{bmatrix} \boldsymbol{x}(t_k) \\ \boldsymbol{T}(t_k) \\ \boldsymbol{e}(t_k) \\ \begin{bmatrix} \boldsymbol{a}_{L1(k)} \\ \boldsymbol{a}_{L2(k)} \end{bmatrix} \end{bmatrix} = \begin{bmatrix} z_{x(k)} \\ z_{T(k)} \\ z_{e(k)} \\ z_{a(k)} \end{bmatrix} - \begin{bmatrix} n_{x(k)} \\ n_{T(k)} \\ n_{e(k)} \\ n_{a(k)} \end{bmatrix} \tag{20}$$

This information equation can be used to determine float-ambiguity estimates of $\boldsymbol{x}(t_k)$, $\boldsymbol{T}(t_k)$, $\boldsymbol{e}(t_k)$, and $[\boldsymbol{a}_{L1(k)};\boldsymbol{a}_{L2(k)}]$ by setting the noise vectors $n_{x(k)}$, $n_{T(k)}$, $n_{e(k)}$, and $n_{a(k)}$ equal to zero and inverting the large square-root information matrix on the left-hand side, but these estimates are not optimal if the double-differenced carrier phase ambiguities are known to take on integer values. The lower two lines of this system of 4 coupled equations constitute the *a priori* information about $\boldsymbol{e}(t_k)$ and $[\boldsymbol{a}_{L1(k)};\boldsymbol{a}_{L2(k)}]$ that is needed for propagation forward to sample time t_{k+1}. This information enables the SRIF algorithm to execute recursively.

D. Estimation of Double-Differenced Ambiguities as Integers Using a LAMBDA Method

Improved estimates of all unknowns can be obtained if double differences between elements of the vector $[\boldsymbol{a}_{L1(k)};\boldsymbol{a}_{L2(k)}]$ can be resolved as exact integers. This integer resolution procedure operates by transforming the ambiguities in a way that splits them between double-differenced integer values and irreducibly real values. This transformation is developed by first considering the index sets $S_{A(k)}$, $S_{B(k)}$, and $S_{com(k)}$. Suppose that $n_{com(k)} > 1$.

Then the index set $S_{com(k)}$ and its mappings into the elements of $\boldsymbol{a}_{L1(k)}$ and $\boldsymbol{a}_{L2(k)}$ can be used to determine the matrix $D_{(k)}$ that forms the vector of all independent integer-valued double-differences between elements of $\boldsymbol{a}_{L1(k)}$ or $\boldsymbol{a}_{L2(k)}$:

$$\boldsymbol{N}_{(k)} = \begin{bmatrix} D_{(k)}\boldsymbol{a}_{L1(k)} \\ D_{(k)}\boldsymbol{a}_{L2(k)} \end{bmatrix} \tag{21}$$

The dimension of the double-differenced vector $\boldsymbol{N}_{(k)}$ is $2[n_{com(k)}\text{-}1]$, and the dimension of the double-differencing operator matrix $D_{(k)}$ is $[n_{com(k)}\text{-}1]$-by-$[n_{A(k)}+n_{B(k)}]$. Each row of $D_{(k)}$ has all zero values except for two -1 values and two +1 values. One of the -1 values occurs in the column associated with receiver A's carrier phase ambiguity for the first SVID in $S_{com(k)}$, and one of the +1 values occurs in the column that maps to the corresponding ambiguity for receiver B. The other +1 value in row i occurs in the column that maps to receiver A's carrier phase ambiguity for the $(i+1)^{st}$ SVID in $S_{com(k)}$, and the other -1 value in row i occurs in the column that maps to the same ambiguity for receiver B.

The $D_{(k)}$ matrix is used to develop a transformation that splits $\boldsymbol{a}_{L1(k)}$ and $\boldsymbol{a}_{L2(k)}$ into their irreducibly real and double-differenced integer components. This development starts with the following QR factorization:

$$Q_{4(k)}\begin{bmatrix} R_{4(k)} \\ 0 \end{bmatrix} = D_{(k)}^{\mathrm{T}} \tag{22}$$

where $Q_{4(k)}$ is an orthonormal matrix and $R_{4(k)}$ is a square, upper-triangular, non-singular matrix. These matrices are used to form the square, non-singular $[n_{A(k)}+n_{B(k)}]$-by-$[n_{A(k)}+n_{B(k)}]$ transformation matrix

$$E_{(k)} = Q_{4(k)}\begin{bmatrix} 0 & \{R_{4(k)}^{-1}\}^{\mathrm{T}} \\ I & 0 \end{bmatrix} \tag{23}$$

This transformation can then be used to express the vector $[\boldsymbol{a}_{L1(k)};\boldsymbol{a}_{L2(k)}]$ in the following form:

$$\begin{bmatrix} \boldsymbol{a}_{L1(k)} \\ \boldsymbol{a}_{L2(k)} \end{bmatrix} = \begin{bmatrix} E_{(k)}\begin{bmatrix} I & 0 & 0 & 0 \\ 0 & 0 & I & 0 \end{bmatrix} \\ E_{(k)}\begin{bmatrix} 0 & I & 0 & 0 \\ 0 & 0 & 0 & I \end{bmatrix} \end{bmatrix} \begin{bmatrix} \begin{bmatrix} \boldsymbol{a}_{irL1(k)} \\ \boldsymbol{a}_{irL2(k)} \end{bmatrix} \\ \begin{bmatrix} \boldsymbol{N}_{L1(k)} \\ \boldsymbol{N}_{L2(k)} \end{bmatrix} \end{bmatrix} = \begin{bmatrix} F_{ir(k)} & F_{N(k)} \end{bmatrix} \begin{bmatrix} \boldsymbol{a}_{ir(k)} \\ \boldsymbol{N}_{(k)} \end{bmatrix} \tag{24}$$

The vector $\boldsymbol{a}_{ir(k)} = [\boldsymbol{a}_{irL1(k)};\boldsymbol{a}_{irL2(k)}]$ contains the irreducibly real carrier phase ambiguities; it is composed of the irreducibly real L1 and L2 ambiguity vectors $\boldsymbol{a}_{irL1(k)}$ and $\boldsymbol{a}_{irL2(k)}$. The vector of double-differenced ambiguities $\boldsymbol{N}_{(k)} = [\boldsymbol{N}_{L1(k)};\boldsymbol{N}_{L2(k)}]$ is composed of the L1 and L2 double-differenced ambiguity vectors $\boldsymbol{N}_{L1(k)}$ and $\boldsymbol{N}_{L2(k)}$.

The transformation matrices $F_{ir(k)}$ and $F_{N(k)}$, which are defined in terms of $E_{(k)}$ in accordance with eq. (24), can be used to transform the last line of the system of coupled information equations in eq. (20). This information equation can then be QR-factorized in order to isolate the integer ambiguities from the irreducibly real ambiguities. This QR factorization takes the form:

$$Q_{5(k)}\begin{bmatrix} R_{irir(k)} & R_{irN(k)} \\ 0 & R_{NN(k)} \end{bmatrix} = \begin{bmatrix} R_{aa(k)}F_{ir(k)} & R_{aa(k)}F_{N(k)} \end{bmatrix} \tag{25}$$

where $Q_{5(k)}$ is an orthonormal matrix, $R_{irir(k)}$ and $R_{NN(k)}$ are square, upper-triangular, non-singular matrices, and $R_{irN(k)}$ is a matrix of appropriate dimensions. The transformation of the information equation is completed by forming the vectors $\boldsymbol{z}_{ir(k)}$ and $\boldsymbol{z}_{N(k)}$ using the formula

$$\begin{bmatrix} \boldsymbol{z}_{ir(k)} \\ \boldsymbol{z}_{N(k)} \end{bmatrix} = Q_{5(k)}^{\mathrm{T}}\,\boldsymbol{z}_{a(k)} \tag{26}$$

The following auxiliary transformations help in the computation of the estimates of other quantities and in the computation of the estimation error covariance matrix:

$$\begin{bmatrix} R_{xir(k)} & R_{xN(k)} \\ R_{Tir(k)} & R_{TN(k)} \\ R_{eir(k)} & R_{eN(k)} \end{bmatrix} = \begin{bmatrix} R_{xa(k)} \\ R_{Ta(k)} \\ R_{ea(k)} \end{bmatrix} \begin{bmatrix} F_{ir(k)} & F_{N(k)} \end{bmatrix} \tag{27}$$

The resulting transformations isolate an independent square-root information equation for the double-differenced ambiguity vector $\boldsymbol{N}_{(k)}$. This equation can be used to define the following integer least-squares cost function:

$$J[\boldsymbol{N}_{(k)}] = \tfrac{1}{2}[R_{NN(k)}\boldsymbol{N}_{(k)}\text{-}\boldsymbol{z}_{N(k)}]^{\mathrm{T}}[R_{NN(k)}\boldsymbol{N}_{(k)}\text{-}\boldsymbol{z}_{N(k)}] \tag{28}$$

The optimal integer-valued minimizer to the cost function in eq. (28) is determined using the LAMBDA pre-conditioning transformation and the integer least-squares solution algorithm of Ref. 18. Suppose that this optimal estimate is $\hat{\boldsymbol{N}}_{(k)}$. It is used in a back-substitution process to determine the estimates of the remaining unknowns. These estimates are

$$\hat{\boldsymbol{a}}_{ir(k)} = R_{irir(k)}^{-1}[\boldsymbol{z}_{ir(k)} - R_{irN(k)}\hat{\boldsymbol{N}}_{(k)}] \tag{29a}$$

$$\hat{\boldsymbol{e}}(t_k) = R_{ee(k)}^{-1}[\boldsymbol{z}_{e(k)} - R_{eir(k)}\hat{\boldsymbol{a}}_{ir(k)} - R_{eN(k)}\hat{\boldsymbol{N}}_{(k)}] \tag{29b}$$

$$\hat{\boldsymbol{T}}(t_k) = R_{TT(k)}^{-1}[\boldsymbol{z}_{T(k)} - R_{Te(k)}\hat{\boldsymbol{e}}(t_k) - R_{Tir(k)}\hat{\boldsymbol{a}}_{ir(k)} - R_{TN(k)}\hat{\boldsymbol{N}}_{(k)}] \tag{29c}$$

$$\hat{\boldsymbol{x}}(t_k) = R_{xx(k)}^{-1}[\boldsymbol{z}_{x(k)} - R_{xT(k)}\hat{\boldsymbol{T}}(t_k) - R_{xe(k)}\hat{\boldsymbol{e}}(t_k) - R_{xir(k)}\hat{\boldsymbol{a}}_{ir(k)} - R_{xN(k)}\hat{\boldsymbol{N}}_{(k)}] \tag{29d}$$

The information equations can also be used to develop an

estimation error covariance matrix for the real-valued estimation vector $\hat{\boldsymbol{x}}_{r(k)} = [\,\hat{\boldsymbol{x}}(t_k)\,;\hat{\boldsymbol{T}}(t_k)\,;\hat{\boldsymbol{e}}(t_k)\,;\hat{\boldsymbol{a}}_{ir(k)}\,]$. It is $P_{rr(k)} = R_{rr(k)}^{-1}[R_{rr(k)}^{-1}]^{\mathrm{T}}$ where

$$R_{rr(k)} = \begin{bmatrix} R_{xx(k)} & R_{xT(k)} & R_{xe(k)} & R_{xir(k)} \\ 0 & R_{TT(k)} & R_{Te(k)} & R_{Tir(k)} \\ 0 & 0 & R_{ee(k)} & R_{eir(k)} \\ 0 & 0 & 0 & R_{irir(k)} \end{bmatrix} \tag{30}$$

Unlike the algorithm of Ref. 7, the current estimation algorithm does not include an integer validation and fixing procedure. This approach creates inefficiencies because double-differenced ambiguities that are essentially known at sample time t_{k-1} must be re-estimated at time t_k. This re-estimation translates into added calculations in the LAMBDA pre-conditioning and integer least-squares solution calculations for sample time t_k. Fortunately, the integer least-squares methods of Ref. 18 execute sufficiently fast to keep this inefficiency from being overly costly in terms of computation time. An advantage of this approach is that it avoids the problem encountered in Ref. 7 of determining a robust integer validation procedure.

IV. TRUTH-MODEL SIMULATION

An off-line truth-model simulation has been developed to test the CDGPS algorithm of Section III. This method of testing is needed because no flight data or hardware simulation data is available for GPS receivers on a pair of high-altitude spacecraft. The simulation that has been used is described in detail in Ref. 13.

The truth-model simulation incorporates many realistic effects. It includes models of transmitter and receiver gain patterns, space loss, transmitted power, and receiver thermal noise. These models are used to calculate the received carrier-to-noise ratio, C/N_0. Minimum acquisition and tracking threshold values of C/N_0 on the L1 and L2 channels are used in order to determine signal availability subject to a maximum constraint of 12 tracked signals per frequency. These signal availability calculations are critical to determining the performance of the estimator at high altitude because it is uncertain how many transmitter side-lobe signals can be tracked at any given location. One weakness of the simulation is that the nulls at the edges of the transmitters' main lobes have been attenuated because the simulation's transmitter antenna model averages actual measured gains over many azimuths at a given elevation in order to form an axisymmetric transmitter gain pattern.

The simulation's ionospheric model is a modified version of the GPS broadcast model. The modification adds an altitude dependence to the latitude/longitude dependence of the electron density profile. This dependence is characterized by 2 different scale heights in two different altitude ranges. The simulation determines each TEC value by numerically integrating the electron density along the corresponding LOS vector.

The model includes a number of realistic errors. Systematic error effects include attitude-dependent models of carrier phase multi-path and of polarization-induced carrier phase wind-up. Also modeled are slowly varying discrepancies between the truth GPS satellite locations and clock corrections and those determined from the broadcast ephemerides. Random thermal errors are included in the pseudo-range and carrier phase measurements. These depend on the received C/N_0 and on the bandwidth of the tracking loops. The thermal noise model for the carrier phase measurement presumes the use of bit aiding in the carrier tracking loops, which allows the coherent accumulation period to be longer than the 0.020 sec data bit period.

The truth-model dynamic propagation uses an orbital simulation with a moderate level of fidelity and a second-order stochastic simulation of receiver clock drift. The orbital propagation model includes a 10^{th}-order Earth gravity model along with Solar and Lunar gravity gradient effects, atmospheric drag, and solar radiation pressure. The receiver clock drift model includes random terms that replicate the short- and long-time-scale effects on an Allan variance plot [22].

The truth-model simulation outputs truth values that can be used in order to evaluate the accuracy of the new estimation algorithm. These include the truth position and velocity states of user spacecraft *A* and *B* along with their truth receiver clock errors. Also output are truth TEC values, truth corrections to the GPS satellite's broadcast position and clock error time histories, and truth double-differenced carrier phase ambiguities.

V. EVALUATION OF ESTIMATOR USING TRUTH-MODEL SIMULATION RESULTS

The new estimator has been evaluated using truth-model simulation data for several representative cases. A long-baseline LEO case has been considered in order to compare its performance with the performance of a competing method that has been tested using actual flight data. Short-baseline cases have been considered at GEO and HEO. They are representative of possible missions. The final case operates at Lunar altitudes with a baseline distance between receivers *A* and *B* that equals the Moon's diameter. The goal of this case is to perform a preliminary evaluation of the efficacy of CDGPS techniques for surveying the relative locations of Lunar Positioning System (LPS) base stations or for tracking the relative locations of orbiting LPS assets.

Each scenario tests the estimator's performance using two values of s^{j}_{DTEC}, the *a priori* standard deviation of each single-differenced TEC. The first value is chosen to be on the order of the maximum single-differenced TEC as

determined from the truth model, and the second value is considerably larger than this. The point of using two values is to compare a nearly optimal value with a conservative one in order to find out whether the conservative value yields a reasonably fast convergence to the true single-differenced TEC and the true carrier phase ambiguities.

The performance of the new estimator is compared with a more traditional kinematic CDGPS algorithm that uses only L1 pseudo-range measurements and double-differenced L1 carrier phase measurements. This alternate estimation algorithm is like the algorithm described in Ref. 14, except that it has been augmented to allow the deletion and addition of GPS satellites as the receiver channels lose old signals and acquire new ones. The point of this comparison is to determine the advantages, if any, of the new estimation algorithm's enhancements, which include the use of dual-frequency measurements and the use of real-valued, un-differenced ambiguities along with double-differenced integer ambiguities.

A. Long Baseline LEO Results

The first comparison case is for a pair of user spacecraft in similar LEO orbits with an apogee of 660 km, a perigee of 645 km, and an inclination of 87.1 deg. Their separation ranges from 133.8 to 135.4 km and is mostly in the along-track direction. The GPS receivers use a patch antenna with a hemispherical gain pattern that is nominally pointed towards zenith, and they use an elevation mask angle of 5 deg measured with respect to their patch antenna's horizon. User spacecraft *A* tracks between 7 and 11 GPS signals during a single orbit, user spacecraft *B* sees anywhere from 6 to 12 signals, and the number of GPS satellites in common view ranges from 6 to 11. The GPS constellation includes 27 satellites. The nominal sample period for this case is $(t_k - t_{k-1}) = 2$ sec.

Results for this case are presented in Fig. 2, which plots time histories of the components of the relative position error vectors along with the number of commonly visible GPS satellites and their corresponding GDOP value. The top plot shows along-track (A-T) error component time histories for 3 different estimation runs that operate on the same truth-model data, and the second and third plots from the top show the corresponding cross-track (C-T) and altitude (ALT) error component time histories. The solid dark-grey curves are for the new estimator using s^j_{DTEC} = 0.11 TECU, the dash-dotted black curves are for the new estimator with s^j_{DTEC} = 2.00 TECU, and the light-grey dashed curves are for the comparison estimator that uses only L1 data. The bottom plot presents the time histories for the number of GPS signals commonly available to receivers *A* and *B* and the resulting GDOP.

There are large initial error transients for the new estimator when s^j_{DTEC} = 2.00 TECU and for the L1-only comparison estimator, as shown in the top 3 plots of Fig. 2. These correspond to initial errors in the integer ambiguity estimates, as evidenced by the results of Fig. 3. The top plot of Fig. 3 graphs the time histories of the maximum double-differenced carrier phase ambiguity errors for each of the three estimators, and the bottom plot graphs the number of ambiguities that are in error at any given time for the corresponding estimator. The initial error transients on the top three plots of Fig. 2 correspond to times when the two ambiguity error metrics are non-zero. The two figures indicate that the new estimator with s^j_{DTEC} = 0.11 TECU converges to the correct ambiguities on the first sample. The new estimator with s^j_{DTEC} = 2.00 TECU takes 412 sec to determine the correct ambiguities, and the L1-only estimator does not stabilize at the correct ambiguities until it has processed 456 sec of data. The new estimator, when used with the lowest s^j_{DTEC} tuning value, converges the most rapidly, as expected.

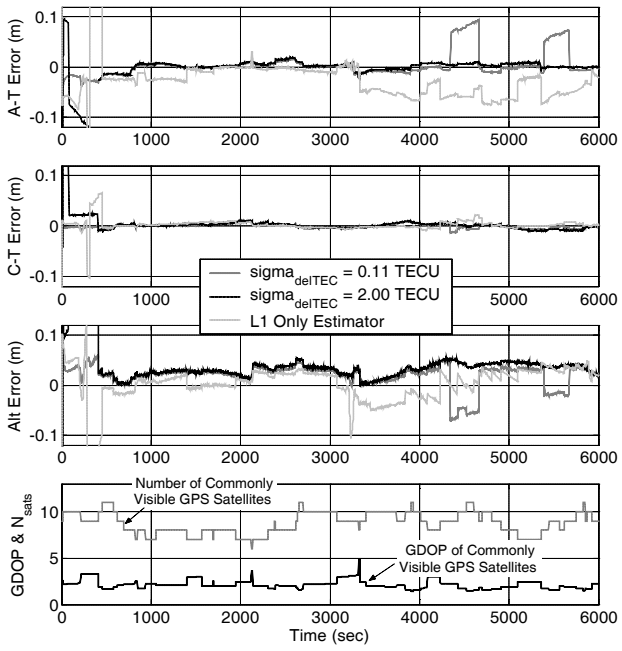

Fig. 2. Time histories of relative position error components, GDOP, and the number of commonly available GPS signals for a long-baseline LEO case.

Another interesting feature of these plots is the trouble that occurs after t = 3000 sec. The L1-only estimator starts to experience larger errors at about t = 3220 sec. The new estimator with s^j_{DTEC} = 0.11 TECU develops errors in its double-differenced integer ambiguities during two extended periods, and these incorrect ambiguities cause corresponding errors in the along-track and altitude components of the relative position vector. These problems are caused by significant non-zero single-

differenced TEC values. They are discussed in more detail below.

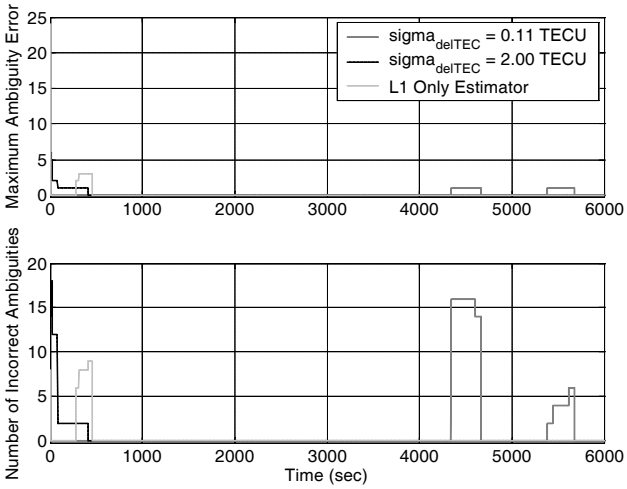

Fig. 3. Two sets of error metric time histories for double-differenced integer ambiguities for a long-baseline LEO case.

The new estimator with s^{j}_{DTEC} = 2.00 TECU has no such troubles. Its ambiguities remain correct, and it experiences no large spikes in its relative position error components, as evidenced in the top three plots of Fig 2. Its peak relative position errors after the initial settling interval are 0.0265 m along-track, 0.0115 m across-track, and 0.0552 m in altitude. These error levels are reasonable given the large baseline and the significant errors due to incorrect GPS broadcast ephemerides and clock corrections. Furthermore, they are consistent with their computed variances as determined using the square-root information matrix of eq. (30).

Further evidence of the efficacy of the new estimator with s^{j}_{DTEC} = 2.00 TECU is presented in Fig. 4. This figure plots the estimated and truth values for the TEC (top plot), the differential TEC (middle plot), and the ECIF X component of the GPS satellite position error when using the broadcast ephemerides to compute position (bottom plot). These plots apply to GPS SVID 1, the top plot is the TEC value along the LOS from receiver *A* to this SVID, and the middle plot is the difference between the TEC values along the lines of sight from receivers *B* and *A* to SVID 1. The top two plots show reasonable tracking performance for the absolute and single-differenced TEC estimates. The bottom plot shows that the estimated correction to the GPS satellite position is not very accurate. Despite the poor convergence of this latter quantity, its inclusion in the filter provides the useful function of informing the estimator about potential low-frequency errors due to uncertainties in the broadcast GPS ephemerides. Note that the GPS position/clock Markov error models for all cases in this paper use the tuning parameters t = 2500 sec and s_e = 0.55 m.

The top plot of Fig. 4 shows a TEC slope discontinuity at about t = 3200 sec, and the middle plot shows a corresponding jump in the differential TEC as the two spacecraft pass through this discontinuity at different times. This discontinuity and similar discontinuities on other channels are what cause the L1-only CDGPS estimator to have an error spike at this time. The middle plot also shows a ramping increase in the differential TEC starting at t = 3500 sec. This increase and similar increases on other channels eventually invalidate the tuning assumption s^{j}_{DTEC} = 0.11 TECU, which is why the corresponding estimator experiences ambiguity errors and relative position error spikes after t = 4000 sec. These increases also explain the degradation of the L1-only estimator's along-track and altitude accuracy during the second half of the orbit.

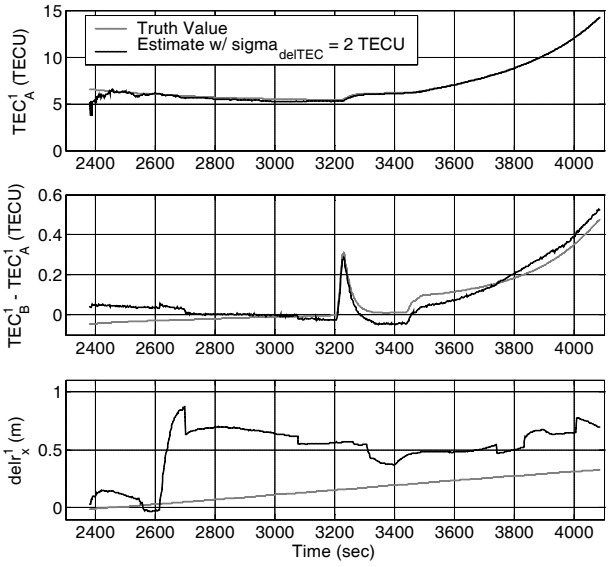

Fig. 4. Truth-value and estimated time histories for representative absolute TEC, single-differenced TEC, and GPS satellite position error for a long-baseline LEO case.

These results can be compared with those of Ref. 7 when operating on actual data from the GRACE mission. The GRACE mission is similar to the present example; it consists of 2 spacecraft orbiting at an altitude of 500 km and an inclination of 89 deg with a separation of about 220 km. Reference 7 implements 2 estimators, one that is kinematic and one that includes dynamic models of the positions, receiver clock errors, and TEC values. The kinematic estimator of Ref. 7 has an accuracy similar to that of this paper's new estimator. Peak along-track errors are on the order of 0.03 m. The dynamics-based estimator of Ref. 7 is more accurate; it achieves peak along-track errors on the order of 0.002 m to 0.007 m. Altitude and cross-track errors are not reported because the "truth" relative position is determined using the GRACE

mission's K-band ranging system, which makes measurements only in the along-track direction. The performance reported in Ref. 7 is for a smoother, which should be more accurate than this paper's new estimator because a smoother uses data from before and after any given time point of interest. Furthermore, the GPS ephemerides used in Ref. 7 are post-processed values that are much more accurate than the broadcast values. Thus, it is surprising and encouraging that the new estimator has performance comparable to that of the Ref.-7 kinematic estimator. It is also encouraging that the new estimator converges to the correct double-differenced integer ambiguities in 412 sec or less while the average convergence time for the Ref.-7 estimator is 1200 sec.

B. GEO Results

A geosynchronous case has been run that uses a short separation of 3 km between receivers *A* and *B*. Their relative position vector is oriented in the along-track direction of their mean orbit. The simulation assumes that both spacecraft carry a typical patch antenna with a hemispherical gain pattern, and that the antenna is nominally pointed towards nadir. It assumes that both GPS receivers have weak-signal acquisition and tracking capabilities which enable them to use L1 signals with carrier-to-noise ratios as low as C/N_0 = 18 dB-Hz and L2 signals with C/N_0 as low as 15 dB-Hz. These levels are feasible given the results of Refs. 9, 10, 11, and 23, but no currently available operational receiver can function at these signal levels. These assumptions about receiver capabilities cause there to be between 11 and 12 GPS signals available at all times. The nominal sample period is $(t_k - t_{k-1})$ = 30 sec for this case.

Results for this case are shown in Fig. 5. This figure is similar to Fig. 2: The top three graphs plot along-track, across-track, and altitude time histories of the relative position error components. The bottom graph plots the number of available GPS satellites common to receivers *A* and *B* and the corresponding GDOP values. Although many satellites are available, GDOP ranges between 7.6 and 13.2 because of their poor geometry; they are clustered relatively near the nadir direction. The top three graphs plot error time histories for 3 estimators, an implementation of the new estimator that uses s^j_{DTEC} = 0.76 TECU, another implementation that uses s^j_{DTEC} = 5.00 TECU, and the L1-only comparison estimator.

The new estimator performs well. The estimator with s^j_{DTEC} = 0.76 TECU converges to the correct double-differenced ambiguities on the first sample, and the s^j_{DTEC} = 5.00 estimator converges in 90 sec. These two estimators have almost identical performance after the initial convergence period. Their peak stead-state error magnitudes are 0.037 m along-track, 0.032 m across-track, and 0.239 m in altitude. The poorer performance in altitude is expected because the high GDOP mostly represents uncertainty of a linear combination of receiver clock error and altitude.

The estimators' predicted relative position error standard deviations have been calculated using the square-root information matrix in eq. (30). Their average values are 0.018 m along-track, 0.015 m across-track, and 0.100 m in altitude. The actual peak errors are commensurate with these standard deviations and bear out the conjecture that the poorer altitude performance is a result of GDOP effects, which are directly reflected in the predicted standard deviations.

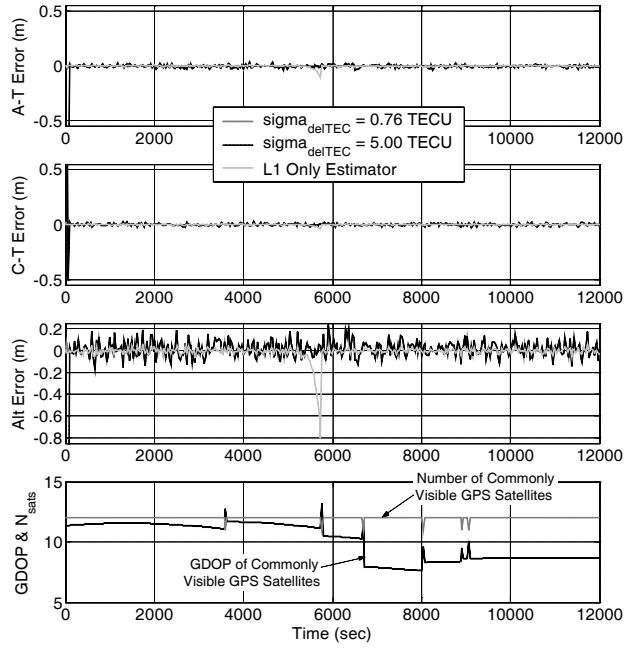

Fig. 5. GEO-case time histories of relative position error components, GDOP, and the number of commonly available GPS signals.

The L1-only comparison estimator performs better than either of the new filters for all times except during the negative altitude error spike that occurs between the times t = 5500 sec and t = 5750 sec. At other times, the along-track, across-track, and altitude peak error magnitudes are, respectively, 0.014 m, 0.008 m, and 0.090 m. The altitude error spike of 0.8 m occurs because the LOS vector to SVID 3 passes very near the Earth. This causes it to cross a long section of increased ionospheric electron density, and the small differences between the LOS vectors to receivers *A* and *B* cause significant differential TEC to develop, which causes the error spike. The new estimators do not have any error spikes because they successfully estimate and remove the spike in the differential TEC.

Thus, the new estimators experience better performance when differential TEC is a concern, but their accuracies

are about 2.5 to 4 times worse when differential TEC is not a concern. This is the expected result because any attempt to estimate additional quantities will increase the estimation error of other quantities if the new estimated quantities are certain to have negligible differences from their *a priori* values and if knowledge of this certainty is withheld from the estimator.

There are two encouraging aspects of the GEO results. First, integer ambiguities can be resolved very rapidly, in 90 sec or less. This occurs even when a large (i.e., conservative) value is used for s^j_{DTEC}. Surprisingly, this occurs even when the peak magnitudes of the relative position error components equal or exceed a carrier wavelength. It is conjectured that integer resolution is possible because there are smaller errors in the sub-space of the estimation problem that contains the double-differenced ambiguities. The second encouraging aspect is the high accuracy of the relative position estimates. Peak component errors of less than 0.25 m can be achieved despite average GDOP values of about 10.

C. HEO Results

A HEO case has been run for a pair of spacecraft in a highly elliptical mean Earth orbit with a perigee altitude of 0.2 Earth radii and an apogee altitude of 17 Earth radii. The separation between the two spacecraft in a representative arc near apogee ranges from 9.3 km to 14.1 km in the along-track direction. These conditions are similar to those described for the Magnetospheric Multiscale Mission [2]. Each spacecraft is assumed to carry a hemispherical patch antenna that is nominally pointed towards nadir along with a weak-signal enabled receiver that can acquire and track L1 signals down to C/N_0 = 12 dB-Hz and L2 signals down to C/N_0 = 9 dB-Hz. These represent ambitious, but possibly realizable performance goals. If this performance is not realizable, than a higher gain antenna can be substituted for the patch antenna, and similar performance can be achieved using a less capable receiver. These assumed sensitivities allow the receivers to track between 7 and 12 common satellites during a 12000 second data arc that uses a nominal sample period of $(t_k - t_{k-1})$ = 30 sec.

Position error and GDOP time histories for this case are graphed in Fig. 6. These results show many similarities to the GEO case, except the errors are larger and the ambiguities take longer to converge to the true values. The larger errors are mostly the results of larger GDOP values. As shown in the figure's bottom plot, GDOP for the satellites common to both receivers ranges from 60 to 260 and has a mean of 120. Again, GDOP primarily represents an error that is a linear combination of altitude and receiver clock offset.

The new estimator that tunes s^j_{DTEC} to 1.6 TECU converges to the correct ambiguities in 240 sec, and the new estimator that uses s^j_{DTEC} = 10.0 TECU converges in 480 sec. The faster convergence of the first tuning case is consistent with what is expected. After the initial convergence, there are three brief periods when the estimator with the first tuning produces wrong double-differenced ambiguity estimates for one SVID. The ambiguity errors equal only 1 carrier cycle in each of these cases. After the initial convergence of the estimator with the second tuning, there are almost 20 short periods during which it produces wrong integer ambiguities for one or two SVIDs. These errors can be as large as 5 carrier cycles. There is no significant correlation between the observed spikes in the relative position error components and the short spikes in the ambiguity errors. It is conjectured that these errors occur in directions of the ambiguity subspace that do not have a significant impact on the relative position error.

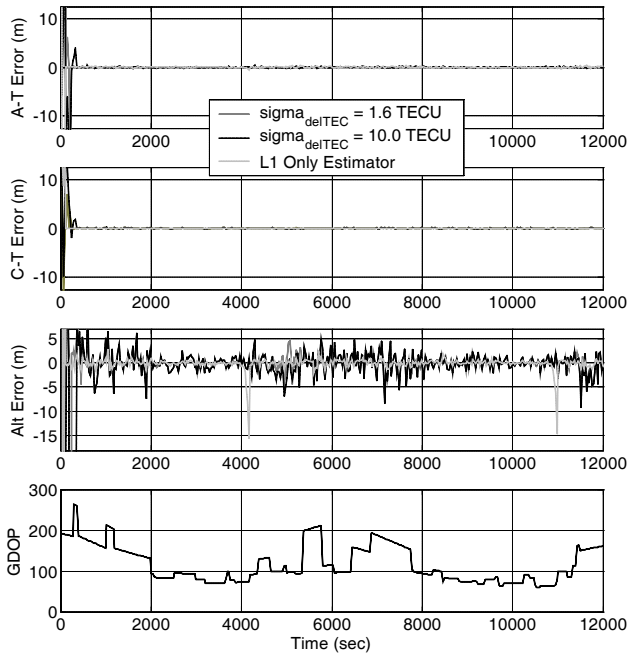

Fig. 6. Relative-position-error and GDOP time histories for a HEO case with an altitude of 17 Earth radii.

As in the GEO case, both cases that use the new estimator show poorer accuracy than the L1-only estimator whenever single-difference TEC is not significant, but the new estimators have superior accuracy when TEC differences become large. This can be seen on the third graph of Fig. 6. The L1-only estimator shows large negative altitude error spikes between the times t = 4000 sec and t = 4200 sec and between the times t = 10800 sec and t = 11000 sec. These correspond to times when one SVID's signal passes near the Earth, and therefore, through a long path of large electron density. At other

times, the L1-only estimator's peak steady-state along-track, across-track, and altitude errors are, respectively, 0.419 m, 0.057 m, and 2.830 m. The corresponding peak steady-state errors for the 2 cases of the new estimator are 0.421 m, 0.257 m, and 8.323 m when s^{j}_{DTEC} = 1.6 TECU and 0.425 m, 0.259 m, and 9.157 m when s^{j}_{DTEC} = 10.0 TECU. The L1-only estimator is about 4.5 times as accurate as the L1/L2 estimator in across-track position, about 3 times as accurate in altitude, and comparable in along-track position when single-differenced TEC is negligible.

The actual error magnitudes for the new estimator are consistent with their computed covariances as determined from the square-root information matrix in eq. (30). This can be seen in a rough way on Fig. 6 by noting that the noisiest sections of the altitude plot tend to correspond to the times when GDOP is the highest -- compare the last two graphs on the figure.

D. Lunar Results

The last case to be considered is for a pair of user spacecraft that are orbiting at the Lunar altitude with an along-track separation of about 3700 km, which is roughly equal to the Lunar diameter. Each receiver is assumed to have a 1 m dish antenna that is pointed towards the Earth and to have the ability track C/N_0 as low as 15 dB-Hz on both the L1 and L2 frequencies. These conditions allow the receivers to track between 10 and 12 common GPS signals, and the achieved GDOP ranges between 650 and 1010 with an average of about 770.

Relative position error and GDOP time histories for this case are shown in Fig. 7. As expected, the relative position errors are larger than in all the other cases, especially in altitude. The errors seem to take about 1000 sec to converge to steady-state performance. Note, however, that the carrier phase double-differenced ambiguities never all converge to correct integer values. During a significant number of samples, the integer least-squares solution algorithm of Ref. 18 terminates prematurely at a sub-optimal solution to the ambiguity resolution problem. It does this because a metric of its computational burden experiences an over-run. This problem is more pronounced for the estimator that uses the higher tuning value of s^{j}_{DTEC}. The poorer accuracy, the incorrect ambiguities when the integer least-squares algorithm does terminate, and the premature termination of the integer least-squares algorithm are all caused by the extremely large GDOP values associated with this case, as depicted in the figure's bottom graph.

Nevertheless, the estimation accuracy of this system is impressive. The steady-state component errors of the new estimator's solution are all smaller than 26 m in magnitude. The new estimators are at least an order of magnitude more accurate than the L1-only estimator – consider the light grey dashed curves that rarely have small enough errors to lie within the vertical bounds of Fig. 7's first and third graphs. If the new algorithm's estimation errors are averaged over the last 11000 sec of this interval, then the relative position error components can be reduced to less than 3 meters. This system might provide a means of surveying the relative positions of base stations of a Lunar Positioning System. Further enhancements, such as knowledge that the receivers are fixed to the Moon, might further improve the accuracy. This type of system warrants further study.

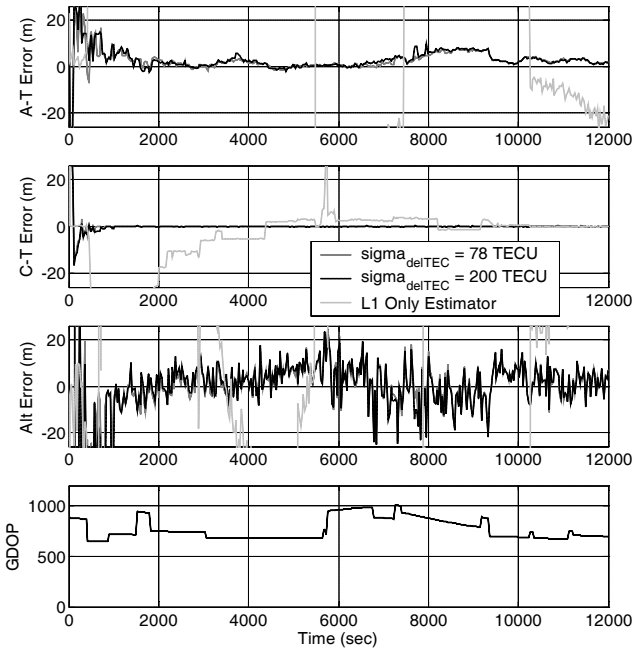

Fig. 7. Relative-position-error and GDOP time histories for a case at the Lunar altitude.

VI. AREAS FOR IMPROVEMENT

There exist a number of possible enhancements that might improve the new estimator. An obvious area for improvement would be to add dynamic models for the absolute and relative positions of receivers *A* and *B*, for the receivers' clock errors, and for the TEC variations [7]. Such models would improve performance by increasing the amount of averaging/filtering of measurement noise. In addition, an orbital dynamic model couples along-track motion to altitude. This coupling would enable the relatively good measurement geometry for determining along-track errors to have a beneficial impact on the large altitude errors. The net effect could be a significant reduction in the equivalent GDOP of the system. As an added benefit, the incorporation of a dynamics model would yield absolute and relative velocity estimates, which would be needed if it were necessary to control the absolute or relative motion of the formation.

A second possible improvement would be to tailor s^j_{DTEC} to use different values for different SVIDs. An SVID with a lower absolute TEC would be assigned a lower standard deviation for the single-differenced TEC, but an SVID with a larger absolute TEC would be assigned a higher standard deviation. For LEO cases, this assignment could be made as a function of the elevation angle of the LOS vector. For high-altitude cases, the assignment could be made as a function of the minimum altitude along the LOS vector. If feasible, this tailoring of s^j_{DTEC} would cause the accuracy of the new estimator to approach that of the L1-only estimator in cases of low single-differenced TEC because the corresponding low s^j_{DTEC} values would signal to the estimator that the single-differenced TEC was near enough to zero to be safely ignored. Conversely, if the single-differenced TEC were larger, then the corresponding larger s^j_{DTEC} values would warn the algorithm to explicitly estimate the single-differenced TEC value based on L1 and L2 data, which would enable it to avoid the L1-only error spikes that are evidenced in Figs. 5 and 6.

A third possible improvement would be to add an ambiguity validation and fixing procedure. It would allow the integer least-squares solver to work with fewer unknowns, which would speed its execution. This validation strategy should probably be tailored to have the capability to fix only some of the integer ambiguities. A related improvement would be to modify the estimator so that it retained the information contained in a validated double-differenced integer ambiguity even when GPS signals associated with that ambiguity were no longer available.

A fourth possible improvement would be to detect and correct for cycle slips. This ability would be particularly important when operating on weak side-lobe signals at high altitudes because the carrier tracking phase-lock loop would have a greater tendency to experience cycle slips. The goal should be to do some sort of hypothesis testing, as in Ref. 14. The necessary algorithm would probably be simpler than that used in Ref. 14 because it should be easier to isolate cycle slips when using un-differenced ambiguities, as in the present formulation.

Additional work should be done to test the ideas presented here. This work should include additional simulation testing and testing with actual flight data. The simulation testing should consider more cases, it should incorporate a model of cycle slips for weak signal cases, and it should use improved transmitter antenna gains patterns that have realistic nulls at the edges of the main lobes. Testing with flight data would need to be restricted to LEO cases because high-altitude data of sufficient quality is not currently available. A prime candidate for testing is the GRACE data that has been used in Ref. 7.

VII. SUMMARY AND CONCLUSIONS

A new estimator has been developed that uses CDGPS techniques in order to determine the relative positions of a pair of Earth-orbiting spacecraft. The estimator uses civilian GPS L1 and L2 pseudo-range and carrier phase data, and it is based on the kinematic approach. It estimates absolute and relative positions, receiver clock corrections, ionospheric TEC, residual errors in the GPS satellite positions and clock corrections, and carrier phase ambiguities. The estimator deals with the ambiguities in a two-stage process. The first stage deals with un-differenced, real-valued ambiguities and performs traditional measurement updates. The second stage uses double-differences to isolate a subspace of the ambiguities that take on exact integer values. A LAMBDA method and an integer least-squares solution are implemented in this sub-space in order to optimally estimate these integers. An additional feature of the estimator is that it uses a pseudo-measurement of the single-differenced ionospheric TEC in order to provide a kind of soft bound on the ambiguity search space. Additional soft bounds to the ambiguity search are provided by the pseudo-range measurements.

The performance of the new estimator has been evaluated using a truth-model simulation. Its long-baseline LEO performance is comparable with that of other kinematic estimators. It has also been tested at altitudes above the GPS constellation, including GEO, an altitude of 17 Earth Radii, and the Lunar altitude. These high-altitude tests presume the availability of GPS receivers that can acquire and track weak side-lobe signals; otherwise, the number of tracked satellites would be insufficient to enable the use of CDGPS techniques. Accuracy is directly affected by the high GDOP values that occur in all high-altitude cases. These values range from about 10 at GEO to near 1000 at the Lunar altitude. Ambiguity resolution happens almost immediately for a short-baseline GEO case, and the maximum relative position error is on the order of 0.25 m. At 17 Earth radii, ambiguity resolution can require as long as 500 sec, and several channels can experience intermittent ambiguity resolution errors if the single-differenced TEC pseudo-measurement bounds are not sufficiently tight. Relative position accuracy in this case is on the order of 10 m. At Lunar altitudes, it becomes difficult to resolve ambiguities correctly, and relative position errors can be as large as 25 m for a baseline equal to the Lunar diameter.

Ambiguity resolution is often possible even when the relative position errors are larger than a carrier wavelength. This result is thought to be caused by a lower uncertainty in the subspace of the estimation problem that is spanned by the double-differenced integer ambiguities. Alternatively, this result may be more a function of the use of a powerful integer least-squares solution algorithm.

ACKNOWLEDGEMENTS

This work has been supported in part by NASA Goddard Space Flight Center through cooperative agreement no. NCC5-722, with Michael Moreau as the agreement monitor, and through a NASA Graduate Student Researcher Program Fellowship, with Russell Carpenter as the fellowship monitor.

REFERENCES

1. Leitner, J., Bauer, F., Folta, D., Carpenter, R., Moreau, M., and How, J., "Formation Flight in Space," *GPS World*, Vol. 13, No. 2, Feb. 2002, pp. 22-31.
2. Gramling, C., Carpenter, R., Lee, T., and Long, A., "Relative Navigation Strategies for the Magnetospheric Multiscale Mission," *Proceedings of the 18th Intn'l. Symposium on Space Flight Dynamics*, Oct. 11-15, 2004, Munich, Germany, http://www.issfd.dlr.de/papers/P1106.pdf.
3. Busse, F.D., How, J.P., and Simpson, J., "Demonstration of Adaptive Extended Kalman Filter for Low-Earth-Orbit Formation Estimation Using CDGPS," *Navigation*, Vol. 50, No. 2, Summer 2003, pp. 79-93.
4. Ebinuma, T., Bishop, R.H., and Lightsey, E.G., "Integrated Hardware Investigations of Precision Spacecraft Rendezvous Using the Global Positioning System," *Journal of Guidance, Control, and Dynamics*, Vol. 26, No. 3, May-June 2003, pp. 425-433.
5. Leung, S., and Montenbruck, O., "Real-Time Navigation of Formation-Flying Spacecraft Using Global-Positioning-System Measurements," *Journal of Guidance, Control, and Dynamics*, Vol. 28, No. 2, March-April, 2005, pp. 226-235.
6. Wolfe, J.D., and Speyer, J.L., "Effective Estimation of Relative Positions in Orbit Using Differential Carrier-Phase GPS," AIAA Paper No. 2004-4777, *Proceedings of the AIAA Guidance, Navigation, and Control Conf.*, August 16-19, 2004, Providence, Rhode Island.
7. Kroes, R., Montenbruck, O., Bertiger, W., and Visser, P., "Precise GRACE Baseline Determination Using GPS," *GPS Solutions*, Vol. 9, No. 1, April 2005, pp. 21-31.
8. Carpenter, J.R., "Lunar Navigation with Libration Point Orbiters and GPS," *The Institute of Navigation Newsletter*, Vol. 14, No. 3, Fall 2004, pp. 6, 7, and 18.
9. Psiaki, M.L., "Block Acquisition of Weak GPS Signals in a Software Receiver," *Proceedings of the ION GPS 2001*, Sept. 11-14, 2001, Salt Lake City, Utah, pp. 2838-2850.
10. Psiaki, M.L., and Jung, H., "Extended Kalman Filter Methods for Tracking Weak GPS Signals," *Proceedings of the ION GPS 2002*, Sept. 24-27, 2002, Portland OR, pp. 2539-2553.
11. Psiaki, M.L., "FFT-Based Acquisition of GPS L2 Civilian CM and CL Signals," *Proceedings of the ION GNSS 2004*, Sept. 21-24, 2004, Long Beach, CA, pp. 457-473.
12. Winternitz, L., Moreau, M., Boegner, G.J. Jr., and Sirotzky, S., "Navigator GPS Receiver for Fast Acquisition and Weak Signal Space Applications," *Proceedings of the ION GNSS 2004*, Sept. 21-24, 2004, Long Beach, CA, pp. 1013-1026.
13. Psiaki, M.L., and Mohiuddin, S., "Modeling, Analysis, and Simulation of GPS Carrier Phase for Spacecraft Relative Navigation," *Proceedings of the AIAA Guidance, Navigation, and Control Conf.*, Aug. 15-18, 2005, San Francisco, CA.
14. Mohiuddin, S., and Psiaki, M.L., "Satellite Relative Navigation Using Carrier-Phase Differential GPS with Integer Ambiguities," *Proceedings of the AIAA Guidance, Navigation, and Control Conf.*, Aug. 15-18, 2005, San Francisco, CA.
15. Odijk, D., "Weighting Ionospheric Corrections to Improve Fast GPS Positioning Over Medium Distance," *Proceedings of the ION GPS 2000*, Sept. 19-22, 2000, Salt Lake City, UT, pp. 1113-1123.
16. Richert, T., and El-Sheimy, N., "Ionospheric Modeling: The Key to GNSS Ambiguity Resolution," *GPS World*, Vol. 16, No. 6, June 2005, pp. 35-40.
17. Teunissen, P.J.G., "The Least-Squares Ambiguity Decorrelation Adjustment: A Method for Fast GPS Integer Ambiguity Estimation." *Journal of Geodesy*, Vol. 70, Nos. 1-2, Nov. 1995, pp. 65-82.
18. Psiaki, M.L., and Mohiuddin, S., "GPS Integer Ambiguity Resolution Using Factorized Least-Squares Techniques," *Proceeding of the Flight Mechanics Symposium*, Oct. 18-20, 2005, NASA Goddard Space Flight Center, Greenbelt, MD.
19. Bierman, G.J., *Factorization Methods for Discrete Sequential Estimation*, Academic Press, (New York, 1977), pp. 69-76, 115-122.
20. Psiaki, M.L., "Null-Space Square-Root Information Filtering and Smoothing for Singular Problems," *Proceeding of the AIAA Guidance, Navigation, and Control Conf.*, Aug. 15-18, 2005, San Francisco, CA; to appear in the *Journal of Guidance, Control, and Dynamics*.
21. Gill, P.E., Murray, W., and Wright, M.H., *Practical Optimization*, Academic Press, (New York, 1981), pp. 37-40.
22. Brown, R.G., and Hwang, P.Y.C., *Introduction to Random Signals and Applied Kalman Filtering, 3rd Edition*, J. Wiley & Sons, (New York, 1997), pp. 428-432.
23. Humphreys, T.E., Psiaki, M.L., Ledvina, B.M., and Kintner, P.M., "GPS Carrier Tracking Loop Performance in the Presence of Ionospheric Scintillations," *Proceedings of the ION GNSS 2005*, Sept. 13-16, 2005, Long Beach, CA.